Advances in Nano Research, *Vol. 13, No.6 (2022) 575-585*
https://doi.org/10.12989/anr.2022.13.6.575

Fe_3O_4 magnetic nanoparticles provide a novel alternative strategy for *Staphylococcus aureus* bone infection

Youliang Ren[†1], Jin Yang[†1], Jinghui Zhang[2], Xiao Yang[1], Lei Shi[1], Dajing Guo[3], Yuanyi Zheng[4], Haitao Ran[5], Zhongliang Deng[*1] and Lei Chu[**1]

[1]*Department of Orthopaedics, Second Affiliated Hospital of Chongqing Medical University, 76 Linjiang Road, Yuzhong Distinct, Chongqing, 400010, P. R. China*
[2]*Key Laboratory of Diagnostic Medicine designated by the Ministry of Education, Department of Laboratory Medicine, Chongqing Medical University Chongqing, Yuzhong Distinct, 400016, P. R. China*
[3]*Department of Radiology, The Second Affiliated Hospital of Chongqing Medical University, 76 Linjiang Road, Yuzhong Distinct, Chongqing, 400010, P. R. China*
[4]*Shanghai Institute of Ultrasound in Medicine, Shanghai Jiao Tong University Affiliated Sixth People's Hospital, 600 Yishan Road, Xuhui Distinct, Shanghai, 200233, P. R. China*
[5]*Chongqing Key Laboratory of Ultrasound Molecular Imaging, Second Affiliated Hospital of Chongqing Medical University, 76 Linjiang Road, Yuzhong Distinct, Chongqing, 400010, P. R. China*

(*Received December 14, 2021, Revised June 16, 2022, Accepted June 17, 2022*)

Abstract. Due to its biofilm formation and colonization of the osteocyte-lacuno canalicular network (OLCN), Staphylococcus aureus (S.aureus) implant-associated bone infection (SIABI) is difficult to cure thoroughly, and may occur recurrently subsequently after a long period dormant. It is essential to explore an alternative therapeutic strategy that can eradicate the pathogens in the infected foci. To address this, the polymethylmethacrylate (PMMA) bone cement and Fe3O4 nanoparticles compound cylinder were developed as implants based on their size and mechanical properties for the alternative magnetic field (AMF) induced thermal ablation, The PMMA mixed with optimized 2% Fe_3O_4 nanoparticles showed an excellent antibacterial efficacy in vitro. It was evaluated by the CFU, CT scan and histopathological staining on a rabbit 1-stage transtibial screw model. The results showed that on week 7, the CFU of infected soft tissue and implants, and the white blood cells (WBCs) of the PMMA+2% Fe_3O_4+AMF group decreased significantly from their controls ($p<0.05$). PMMA+2% Fe_3O_4+AMF group did not observe bone resorption, periosteal reaction, and infectious reactive bone formation by CT images. Further histopathological H&E and Gram Staining confirmed there was no obvious inflammatory cell infiltration, neither pathogens residue nor noticeably burn damage around the infected screw channel in the PMMA+2% Fe_3O_4+AMF group. Further investigation of nanoparticle distributions in bone marrow medullary and vital organs of heart, liver, spleen, lung, and kidney. There were no significantly extra Fe_3O_4 nanoparticles were observed in the medullary cavity and all vital organs either. In the current study, PMMA+2% Fe_3O_4+AMF shows promising therapeutic potential for SIABI by providing excellent mechanical support, and promising efficacy of eradicating the residual pathogenic bacteria in bone infected lesions.
Keywords: biofilm; bone infection; Fe_3O_4 magnetic nanoparticles; OLCN; *Staphylococcus aureus*

1. Introduction

Currently, implant-associated bone infection characterized by aggravated infection-induced inflammatory responses and osteolysis, remains a severe challenge in orthopedic practice (Diaz-Ledezma *et al*. 2019). It occurs up to 2–5 % in orthopedic surgery (Li *et al*. 2018), usually acompanies with multiple revisions, poor functionality, health-related outcomes, and significant financial burden to health care systems (Patel *et al*. 2015, Sullivan *et al*. 2017).

Staphylococcus aureus (*S.aureus*) is responsible for the majority of cases (30% to 60%)(Patel *et al*. 2015), with the characteristic of biofilm formation on the surface of foreign material (Saeed *et al*. 2019) and colonization of the osteocyte-lacuno canalicular network (OLCN) (Adjei-Sowah *et al*. 2021, Masters *et al*. 2019). The recurrent and persistent infections usually occurred in approximately 40% of *Staphylococcal* osteomyelitis patients (Kavanagh *et al*. 2018), increasing the difficulty of treating for *S.aureus* implant-associated bone infection (SIABI). Eradicating microorganisms in a biofilm requires much higher antibiotic concentrations than planktonic ones, systematically applied antibiotics mostly do not reach the minimum effective concentration (MEC). Therefore, successful management of SIABI requires long-term antibiotic treatment combined with appropriate surgical intervention and removal of the contaminated implant (Saeed *et al*. 2019). As debridement, antibiotics, irrigation, and retention regimens are usually not standardized, parts of pathogenic bacteria might not be eradicated from infected lesions completely, so SIABI may occur recurrently after long-term dormant. Recent studies showed that once an implant-associated infection occurs,

*Corresponding author, Professor,
E-mail: zhongliang.deng@yahoo.com
**Co-corresponding author, Ph.D.,
E-mail: chulei2380@163.com
† These authors contributed equally to this work

ISSN: 2287-237X (Print), 2287-2388 (Online)

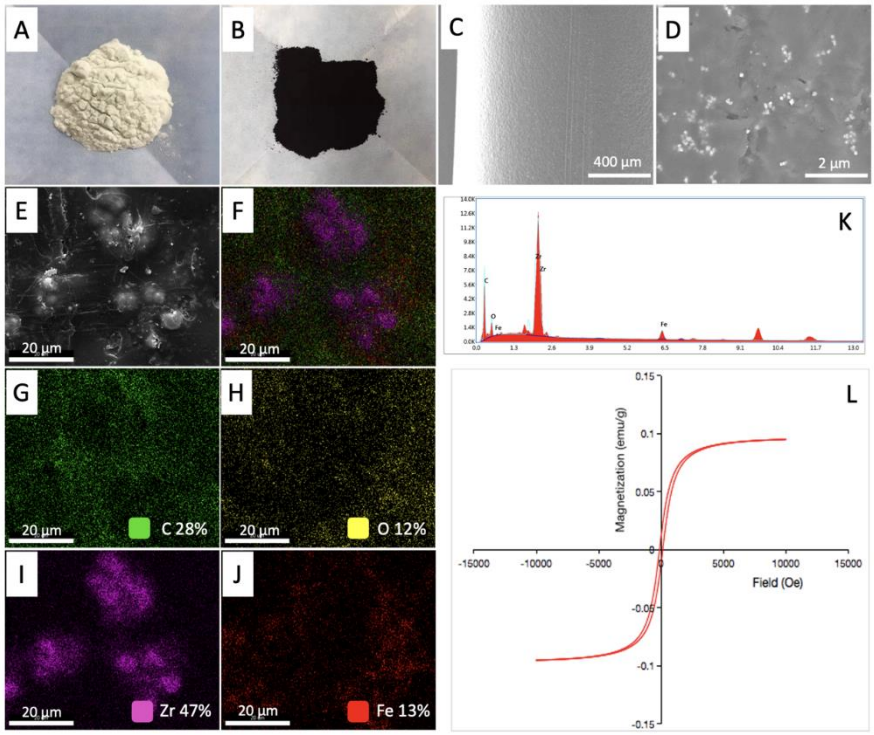

Fig. 1 The Construct Procedure and Energy Dispersive X-ray Spectrometry Analysis of 2%Fe_3O_4 Nanoparticles (NPs)+PMMA Mixture Cylinder. The PMMA powder (A) and Fe_3O_4 NPs (B) were evenly mixed to customize a PMMA+Fe_3O_4 cylindrical module (C). The light microscopy showed the Fe_3O_4 NPs were uniformly distributed in the PMMA powder (D). The energy dispersive X-ray spectrometry (E) was employed to perform the elemental analysis (F-J) and indicated the element percentage of C, O, Zr and Fe were 28% (G), 12% (H), 47% (I) and 13% (J). The atomic percentage of C, O, Zr and Fe were 79.73%, 13.90%, 4.41% and 1.96% and the weight percentage of C, O, Zr and Fe were 56.60%, 13.14%, 23.79% and 6.47%, respectively (K). The hysteresis loops of PMMA+2% Fe_3O_4 were narrow, showing their soft magnetic performance(L)

the rate of reinfection will reach to 40% (Masters *et al*. 2019). Therefore, it is essential to develop a novel therapeutic strategy for SIABI, especially to eradicate the residual pathogenic bacteria thoroughly in bone infected lesions.

Our previous research established the Polymethylmethacrylate (PMMA) bone cement mixed with Fe_3O_4 magnetic nanoparticles has outstanding biomechanical properties of PMMA and the low toxicity of Fe_3O_4 magnetic nanomaterials (Dadfar *et al*. 2019, Liang *et al*. 2020, Yu *et al*. 2019). The compound of PMMA+ Fe_3O_4 showed effectiveness for the treatment of rabbit VX2 tibial plateau tumor ablation exposure to an alternating magnetic field (AMF) (Yu *et al*. 2019), without causing burns to the tissues around the lesion and biological side effects in vivo. Due to its excellent biocompatibility and magnetic properties, the iron oxide nanoparticles (IONPs) have been broadly used in biomedical research (Liu *et al*. 2013). Nowadays, the magnetic iron oxide (Fe_3O_4) nanoparticles have already been approved by the US Food and Drug Administration (FDA) for medical use (Tian *et al*. 2018). Importantly, the IONPs have also been proved to be non-toxic (Samanta *et al*. 2008, Sun *et al*. 2010). It's not only non-lethal but its by-products can be degraded into iron from the cores and that apparently accumulates in natural iron stores in the body (Weissleder *et al*. 1989). In addition, IONPs have been shown to be antibacterial toward *S.aureus* and inhibit its biofilm formation (Shi *et al*. 2016). Thus, some researchers have utilized it for the treatment of Methicillin-resistant *Staphylococcus aureus* (MRSA) infected osteomyelitis and had effective results (Qiao *et al*. 2020). However, the therapeutic efficacy of Fe_3O_4 nanoparticles for SIAB *in vivo* is still not well discovered, especially its efficacy on biofilm eradication. To end this, we employed a dual-functional compound of PMMA+ Fe_3O_4 nanoparticles under an AMF to evaluate its therapeutic potential for SIABI by using a rabbit model.

2. Materials and methods

A commercially available PMMA bone cement Osteopal® V (Heraeus Medical GmbH, Hanau, Germany) was mixed with Fe_3O_4 magnetic NPs (Lot# CAS:1317-61-9, Chengdu AikeDa Chemical Reagent Co., Ltd., China) as previous described (Leiblein *et al*. 2020, Yu *et al*. 2019). Briefly, the PMMA powder (26 g) was composed of PMMA (14.2 g), zirconium dioxide (11.7 g) and benzoyl peroxide (0.1 g) (Fig 1 A), which well mixed with 722mg Fe_3O_4 NPs (the nanoparticle size =120.60 ±38.95 nm) (Fig 1 B) by grinding and sonication about 30 minutes followed with vortex at 3000 RPM over 120s with a vortex mixer (Vortex.Genie2T, Scientific Industries, Ltd, U.S.A.). And

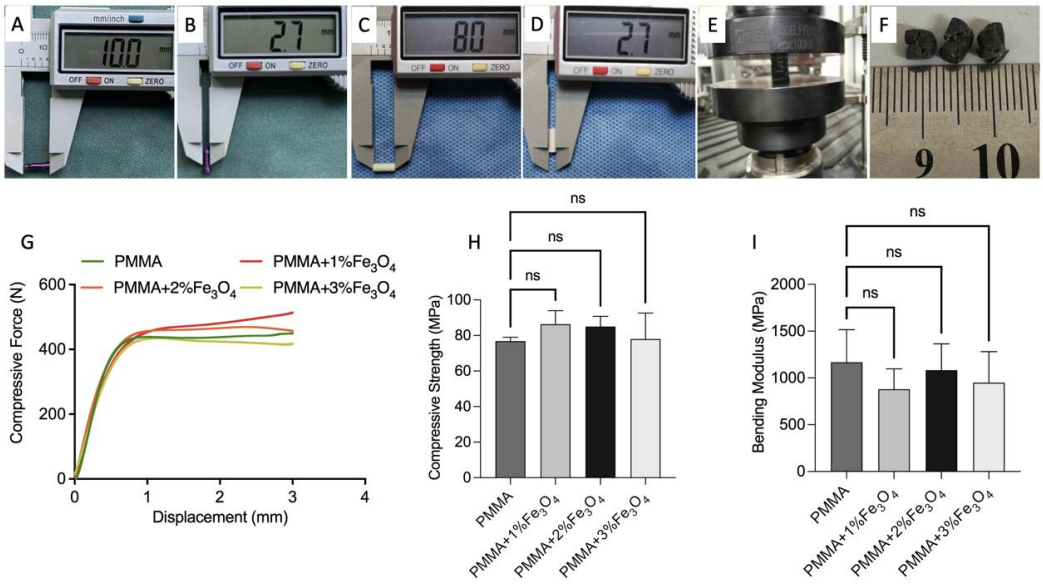

Fig. 2 The Biomechanical Properties of PMMA+Fe_3O_4 Compound Cylinder. The referencing size of titanium screws was adopted *in vivo* (A-B) for standardizing the size of PMMA+Fe_3O_4 cylinder (C-D) for biomechanical testing (E-F) to determine the compressive force, compressive strength, and bending modulus. The compressive force of 1) PMMA was 449.20±2.88N, 2) PMMA+1%Fe_3O_4 was 512.30±2.71N, 3) PMMA+2%Fe_3O_4 was 460.31±3.57N, 4) PMMA+ 3%Fe_3O_4 was 415.43±5.90N (G). The compressive strength of 1) PMMA was 76.8±1.27 MPa, 2) PMMA+1% Fe_3O_4 was 86.37±4.39 MPa, 3) PMMA+2% Fe_3O_4 was 84.97±3.33 MPa, 4) PMMA+3% Fe_3O_4 was 78 ±8.44 MPa (H). The bending modulus of 1) PMMA was 1167.41±201.61 MPa (I), 2) PMMA+1%Fe_3O_4 was 879.98±125.47 MPa, 2) PMMA+1%Fe_3O_4 (879.98±125.47 MPa), 3) PMMA+2%Fe_3O_4 (1083.15±161.92 MPa), and 4) PMMA+3% Fe_3O_4 (949.19 ±191.12 MPa). There was no statistical significance between these groups (1-way ANOVA). (p>0.05). (ns, P>0.05).

then, the PMMA liquid monomer (10 mL) consisted of methyl methacrylate (9.2 g) and N, N-dimethyl-p-toluidine (0.2 g) were added into the powder mixture using 2.0ml sterile Eppendorf tubes. After 1min, the mixture was injected into the cylindrical module (length of 8.00mm and inner diameter of 2.75mm) to establish the standard size of PMMA+Fe_3O_4cylinder (Fig 1 C).

2.1 Morphological characterization and biomechanical properties of PMMA+Fe_3O_4

The microstructure of PMMA+Fe_3O_4 (length of 8.00mm and inner diameter of 2.75mm) was characterized by a field emission scanning electron microscope, FEI INSPECT F50 by FEI Company (America). The elemental analysis was performed by energy dispersive X-ray spectrometry (Figs. 1 E-J). The biomechanical testing was performed by microcomputer of an electronic universal testing machine (Bose, ELF3330, America). Quantum Design North America (PPMS-9) was used for the vibrating sample magnetometer (VSM) (Fig. 2).

2.2 Evaluation of the magnetic-thermal-induced thermal efficiency In vitro

All PMMA+Fe_3O_4 cylinders were exposed to an AMF by a homemade magnetic hyperthermia analyzer (frequency: 626 KHz, output current: 28.6 A, turns of coil: 2, coil length: 1 cm, field amplitude: 5.72 K/Am) for 180 s (Chen *et al*. 2014). Simultaneously, the dynamical changes in temperature of the PMMA+Fe_3O_4 cylinder were recorded by a far-infrared thermometer (FOTRIC225, ZXF Laboratories, U.S.A.) every 10 seconds when the cylinder was exposed to the AMF. The thermal images were analyzed via AnalyzIR 7.1 (ZXF Laboratories, U.S.A.) (Yu *et al*. 2019). To optimize the AMF induced thermal effects, the mixture ratio of Fe_3O_4 for the PMMA+ Fe_3O_4 compound cylinder was set as 1%, 2% and 3% for *in vitro* testing. Based on the outcomes of *in vitro* testing, 2% Fe_3O_4 + PMMA was used for in vivo experimental evaluations.

2.3 Antibacterial properties of PMMA+Fe_3O_4 In vitro

The PMMA+2%Fe_3O_4 (n=3) compound cylinders were sterilized at low temperature using a hydrogen gas plasma sterilizer (LAOKEN LK/MJQ-100) for 58 minutes prior to antibacterial testing. The antibacterial activities of PMMA +2% Fe_3O_4 cylinders were examined by an *S.aureus* (ATCC29213) on tryptic soy broth (TSB) agar plate. The protocol is 1) the mid-logarithmic-phase *S.aureus* bacterial solution was prepared and diluted to 1×10^5 CFU/mL, 2) Add the bacterial solution to the TSB agar plate (diameter of 2.5 cm), 3) The bacterial suspension was swabbed onto the TSB agar plate using a sterilized cotton bud, 4) Next, we inserted the sterilized PMMA+2%Fe_3O_4 cylinder vertically into the center of the TSB agar plate, 5) Placed the plate onto AMF coil, and applied AMF for 180s, 6) then incubated the plate at 37°C overnight, 7) images were

obtained by Scan® 1200 - HD automatic colony counter for antibacterial activity evaluation, and the zone of inhibition were defined as clear zone around the PMMA+Fe_3O_4 cylinder.

2.4 Colony forming units (CFU) assay for infected implants and soft tissue in ex Vivo

On week 1 and 7, the specimens of infected soft tissue and implants were obtained for CFU assay. To extract bacteria for CFU, the soft tissue specimen was placed in a Falcon tube with 2 mL of PBS solution, each infected soft tissue specimen was separately grinded for 45 seconds in a high-throughput tissue grinder (SCIENTZ-4850 Hz). The implant was placed in a Falcon tube with 2ml PBS and sonicated for 15 minutes, and vortexed for 2 minutes. A 10 ul of 1:10 serial dilutions of each specimen were plated to a TSB agar plate incubated at 37℃ overnight for CFU counts.

2.5 Rabbit model of SIABI

All surgical procedures were approved by the Medical Ethics Committee of the Second Affiliated Hospital of Chongqing Medical University. Three groups (n=5/group) of 12 to 14-week-old male New Zealand white rabbits (2-2.5 kg body weight) were anesthetized via intramuscular injection of a mixture of ketamine (25 mg/kg) and xylazine (1.5 mg/kg), and maintained with isoflurane (1.5%).

Sterile titanium screws (length of 10.0mm and diameter of 2.75mm) were immersed in 1×10^5. Colony Forming Units (CFU)/mL *S.aureus* (ATCC29213) bacterial solution overnight and naturally air-dried for 30min before being implanted into the left tibia of rabbits. At week -1 after initial surgery, 1-stage reversion surgery was performed. Briefly, the implantation of *S. aureus* infectious screws was removed from the PMMA+ Fe_3O_4 and PMMA+ Fe_3O_4+AMF groups and followed with wound debridement and irrigation. These two groups were then implanted with a new PMMA+ Fe_3O_4 cylinder as a replacement for additional 7 weeks of follow-up. The untreated group remained without 1-stage reversion surgery.

2.6 Computed tomography images evaluate bone osteolysis

To evaluate the osteolytic bone loss caused by *S. aureus* infection. All rabbits underwent longitudinal weekly computed tomography (CT) scanning for 8 weeks. A 320-slice CT scanner (Aquilion ONE, Canon Medical Systems, Japan) was employed using tube voltage was 100 kV, tube current was 50mA, and the scanning field 220mm with the thickness 0.5mm for all scans. All raw images were used for 3D reconstruction that was performed with the bone algorithm by Canon Medical Systems CT software workstation.

2.7 Histology and serological biomarkers

To confirm CT image findings and further investigate the antibacterial role of PMMA+ Fe_3O_4+AMF, and the systemic biodistributions of biodegraded Fe_3O_4 nano-particles, all tibiae and internal organs (heart, liver, spleen, lung, and kidney) and serum of each individual were harvested for histology and serological test on week 7, Histological staining includes the hematoxylin-eosin (H&E) staining, Gram staining, and Perls Prussian blue staining. Pannoramic DESK, P-MIDI, P250 (3D HISTECH, Hungary) was adapted for scanning the image of histopathological sections. Serological specimens were collected from ear phlebology at indicated time points for white blood cell (WBC) counts and to evaluate the condition of organs preoperative and postoperative (week 7). XT-2000i™ automated hematology analyzers (Sysmex, Japan) was adapted for WBC counts. Alanine aminotransferase (ALT), aspartate aminotransferase (AST), creatinine (CR), blood urea nitrogen (BUN), creatine kinase (CK) and lactate dehydrogenase levels (LDH-L) were tested by Catalyst Dx® Chemistry Analyzer (America).

2.8 Statistical analysis

Data were analyzed by using Prism 9.0 (GraphPad Software, San Diego, CA) and are presented as the mean and standard error of the mean (SEM). Data were analyzed by a 2-tailed Student *t-test*, 1-way ANOVA or 2-way ANOVA. P values of <0.05 were considered significant (ns $p > 0.05$, *$p < 0.05$, ** $p < 0.01$).

3. Results

3.1 Morphological characterization and biomechanical properties of PMMA-Fe_3O_4

As SEM images of PMMA+2%Fe_3O_4 cylinder are shown in Fig. 1A-D, the Fe_3O_4 NPs were uniformly distributed in the PMMA+Fe_3O_4 NPs mixture (Fig. 1D). There was no congregated crystallization or connection between the NPs, indicating that Fe_3O_4 NPs successfully integrated into the PMMA matrix without damaging its original structure. To clarify the component of PMMA+2% Fe_3O_4 which achieved by energy dispersive X-ray spectrometry (Fig. 1E), the elemental analysis of overlay image (Fig. 1F) was performed for different elements, including the element weight percentage of C (Fig. 1G), O (Fig. 1H), Zr (Fig. 1I) and Fe (Fig. 1J), and their atomic percentage (Fig. 1K), and the element mappings exhibited a uniform distribution of ferrous elements with carbonaceous and oxygen frameworks, indicating good dispersity of Fe_3O_4 NPs in the solid phases. The hysteresis loops of PMMA+2% Fe_3O_4 indicates its soft magnetic performance (Fig. 1L). Of note that the microstructure and magnetometer of Fe_3O_4 NPs had been performed in previous studies (Yu *et al*. 2019).

The titanium screws that implanted *in vivo* (Fig. 2and B) were used as a referencing size for PMMA+Fe_3O_4 cylinder (Fig. 2C and D). The biomechanical testing of PMMA+ Fe_3O_4 cylinder (Fig. 2E and F) included compressive force, (Fig. 2G) compressive strength (Fig. 2H) and bending modulus (Fig. 2I), and there was no any significant differences with all of three PMMA+Fe_3O_4 groups. These

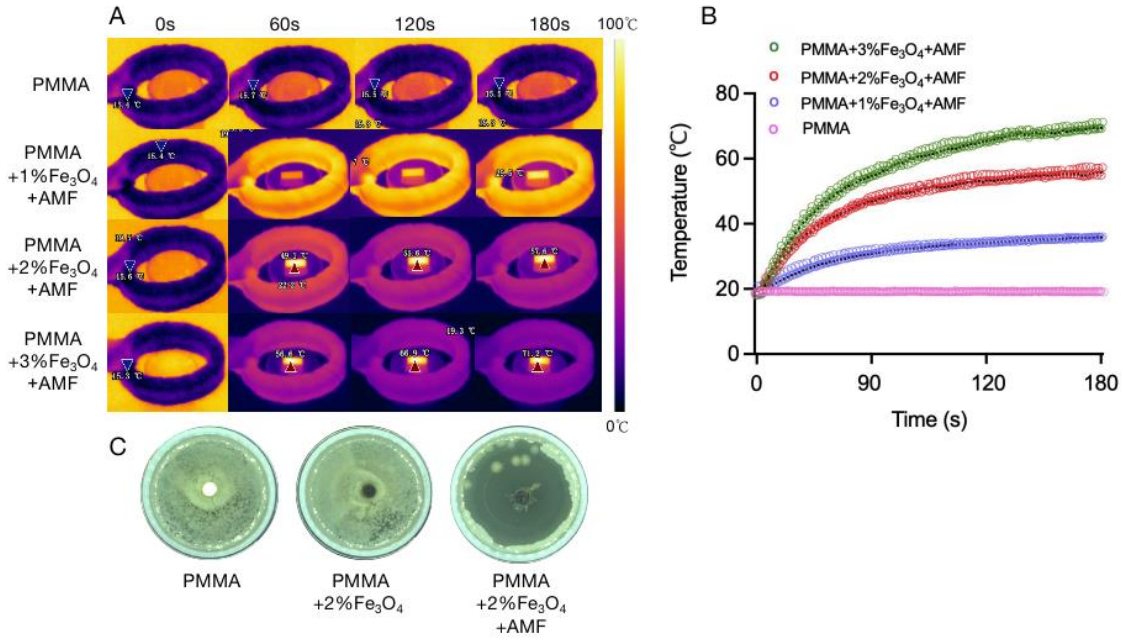

Fig. 3 Magnetic-induced Thermal Efficiency and Antibacterial Properties of PMMA+Fe_3O_4 *In Vitro*. The antibacterial efficacy of PMMA+ Fe_3O_4 was performed in the *S. aureus* TSB agar plate. The PMMA+Fe_3O_4 cylinder was placed in the center of the *S. aureus* saturated TSB agar plate, and exposed to an AMF (PMMA+2% Fe_3O_4+AMF) for 180s. The thermal images were recorded by a far-infrared thermometer (A) and the data was proceed by AnalyzIR (B). Compared with PMMA (19.2±0.07℃), the magnetic induced temperature: 1) PMMA+1%Fe_3O_4+AMF:35.83±0.09℃, 2) PMMA+2%Fe_3O_4+AMF: 56±0.7℃, 3) PMMA+3% Fe_3O_4+AMF: 69.93±0.64℃. The inhibition zone of *S. aureus* TSB agar plate showed the dark green zone when PMMA+2%Fe_3O_4 cylinder exposure to AMF for 180s (C).

results suggested that the proportion of Fe_3O_4 mixed into PMMA+Fe_3O_4 in this study has not significantly changed the biomechanical properties of PMMA itself, this undoubtedly provides an important basis for us to utilize PMMA+Fe_3O_4 for subsequent *in vivo* studies.

3.2 AFM ımages of gold nanoparticles coated on active SERS glass substrates as plasmonic sensors

All PMMA+Fe_3O_4 cylinders were exposed to an AMF by a homemade magnetic hyperthermia analyzer (frequency: 626 KHz, output current: 28.6 A, turns of coil: 2, coil length: 1 cm, field amplitude: 5.72 K/Am) for 180 s (Chen *et al*. 2014). Simultaneously, the dynamical changes in temperature of the PMMA+Fe_3O_4 cylinder were recorded by a far-infrared thermometer (FOTRIC225, ZXF Laboratories, U.S.A.) every 10 seconds when the cylinder was exposed to the AMF. The thermal images were analyzed via AnalyzIR 7.1 (ZXF Laboratories, U.S.A.) (Yu *et al*. 2019). To optimize the AMF induced thermal effects, the mixture ratio of Fe_3O_4 for the PMMA+Fe_3O_4 compound cylinder was set as 1%, 2% and 3% for in vitro testing. Based on the outcomes of *in vitro* testing, 2%Fe_3O_4 + PMMA was used for *in vivo* experimental evaluations.

The thermal images were recorded by far-infrared thermometer after exposing to an AMF for 0s, 60s, 120s, and 180s (Fig. 3A) and the data was analyzed by AnalyzIR (Fig. 3B). The temperature of PMMA+1%Fe_3O_4, PMMA+ 2%Fe_3O_4 and PMMA+3%Fe_3O_4 could reach 35.83±0.09℃, 56±0.7℃, and 69.93±0.64℃, respectively. Obviously, the higher percentage of Fe_3O_4 particles in the PMMA+Fe_3O_4 cylinder can produce higher temperature by increase the generation of heat in the alternating magnetic field (AMF), but too much higher temperature may further cause tissue burn (Fan *et al*. 2019). Thus, considering the results of biomechanical testing, we finally determined use PMMA+ 2%Fe_3O_4 for further antibacterial experimental *in vitro*. Fortunately, the inhibition zone of PMMA+2%Fe_3O_4 cylinder for *S.aureus* in the TSB agar plate is quite appreciable (Fig. 3C).

3.3 In vivo evidence of antibacterial efficiency of PMMA+2%Fe_3O_4 for SIABI rabbit transtibial implant module

By following the experimental schedule (Fig. 4A), we observed that *S.aureus* colonized on the surface of the contaminated implant at week 1 by scanning electron microscopy (SEM) (Fig. 4 $B_{1,2,\ 3,4}$ yellow dish line and arrow) and the biofilm formation of *S.aureus* (Fig. 4 B_4 white arrows). At week 7, CFU of infectious soft tissue in the untreated group ($2.9\times10^7\pm2.8\times10^7$) was significantly higher than the PMMA+Fe_3O_4+AMF group ($9.1\times10^4\pm 6.1\times10^4$) ($p<0.05$), while there was no statistical significant between the untreated group and PMMA+Fe_3O_4 group ($4.3\times10^6\pm4.1\times10^6$) ($p>0.05$) (Fig. 4C). This demonstrated that although debridement and removal of infected implanted could reduce the CFU of bacteria in infected lesions, but it couldn't eradicate the bacteria from adjacent soft tissues thoroughly. In addition, the CFU of infected

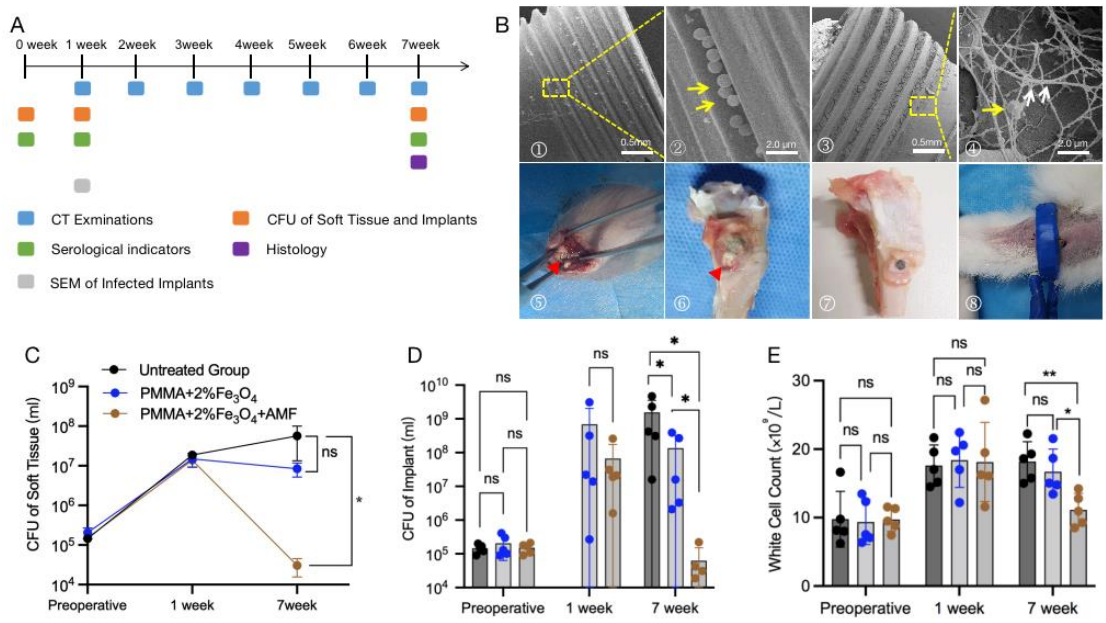

Fig. 4 Excellent Antibacterial Efficiency of PMMA+2%Fe_3O_4 +AMF for SIABI Rabbit Module *In Vivo*. Based on the results from Fig. 3, we used PMMA+2%Fe_3O_4 for *in vivo* testing. The Schematic experiments were scheduled (A). The bacterial loading on the implant screw was checked by SEM at preoperative (B1,2) and 1 week after implanted (B3,4). The surgical implantation of week 0 (B5), week 1(B6), week 7 (B7) and AMF application (B8) are shown. The CFU assay of soft tissue (C) and implant (D) indicated excellent antibacterial efficiency in PMMA+2%Fe_3O_4+ AMF group. But there was no significantly different observed in blood white cell counts (E). (ns, p >0.05, * p<0.05, ** p<0.01).

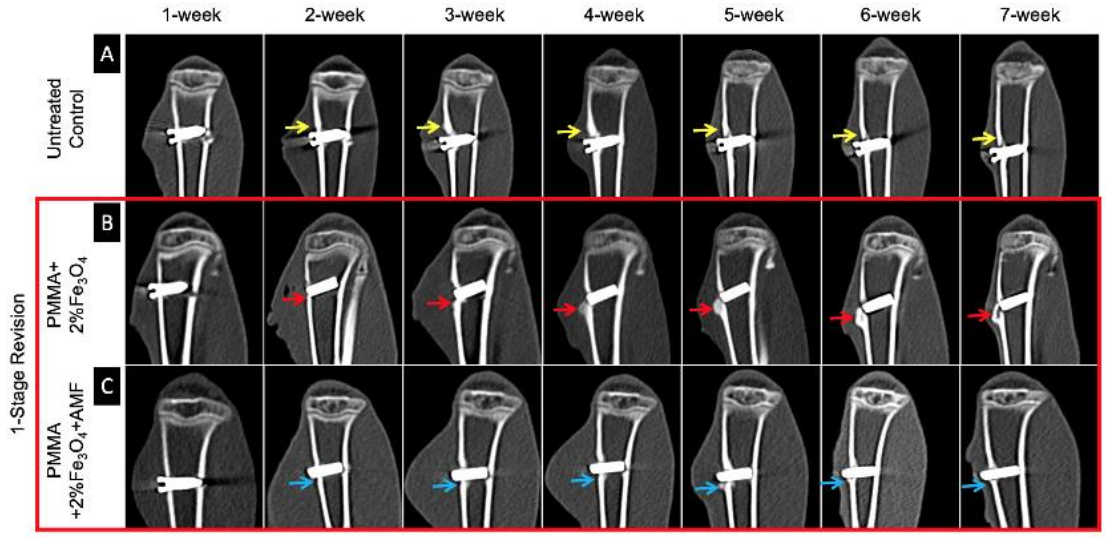

Fig. 5 Longitudinal CT Scan Showed Less Osteolytic Bone Lost and Improved Osteointegration of PMMA+ 2%Fe_3O_4+AMF in SIABI Rabbit 1-stage Reversion Transtibial Implant Model. Representative CT images of untreated group (A) and 1-stage revision of PMMA+ 2%Fe_3O_4 (B) or PMMA+2%Fe_3O_4+AMF (C) showed remarkable cortical bone osteolysis and bone resorption around the infected screw (A, yellow arrows), At the early stage of the PMMA+ Fe_3O_4 group (B, week 4), and the periosteal reaction of the lateral cortex bone around the infected lesions (B, red arrows) from week 4 to 7 after infection, While none of this manifestation could not be found in PMMA+Fe_3O_4+AMF group (C, blue arrows). In addition, this group also shown promising osteointegration adhering to PMMA+Fe_3O_4 cylinder.

implant in the PMMA+2% Fe_3O_4+AMF group was significantly reduced at week 7 (Fig. 4D). At week 7, the WBC of PMMA+Fe_3O_4+AMF group was nearly back to normal level (Fig. 4E). Based on 7 weeks of longitudinally CT follow-up images of SIABI rabbits, those imaging signals that indicate the severity of SIABI could not be observed around the infected screw in PMMA+Fe_3O_4+AMF group obviously (Fig. 5C, blue arrows), like periosteal

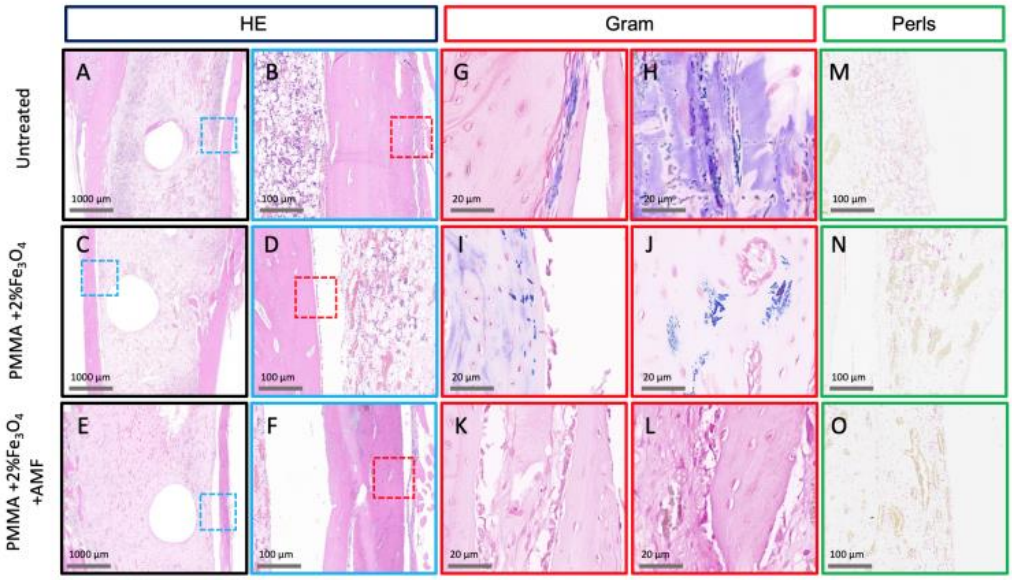

Fig. 6 Histopathological Confirmation of Antibacterial Efficiency of PMMA+ 2% Fe_3O_4+AMF on SIABI Rabbit Module. On week 7, the specimens were processed with sagittal cuts perpendicular to implants and three continue immediately adjacent slides were used for histopathological staining of H&E (A-F, black and blue box), Gram (G-L, red box) and Perls Prussian Blue (M-O, green box). The region of interest for Gram (G-L) and Perls Prussian Blue (M-O) staining were determined from the H&E (dish line box in A, C, E (blue) & B, D, F(red)) and Gram staining of untreated and PMMA+2%Fe_3O_4 groups showed bacteria resident inside of the cortical bone (G, H, and I, J), but not observed in PMMA+2% Fe_3O_4+AMF (K, L). Further, Perls Prussian blue staining showed no iron nanoparticles escaping from PMMA+ Fe_3O_4 compound cylinders to adjacent bone and bone marrow tissues (M, N, O).

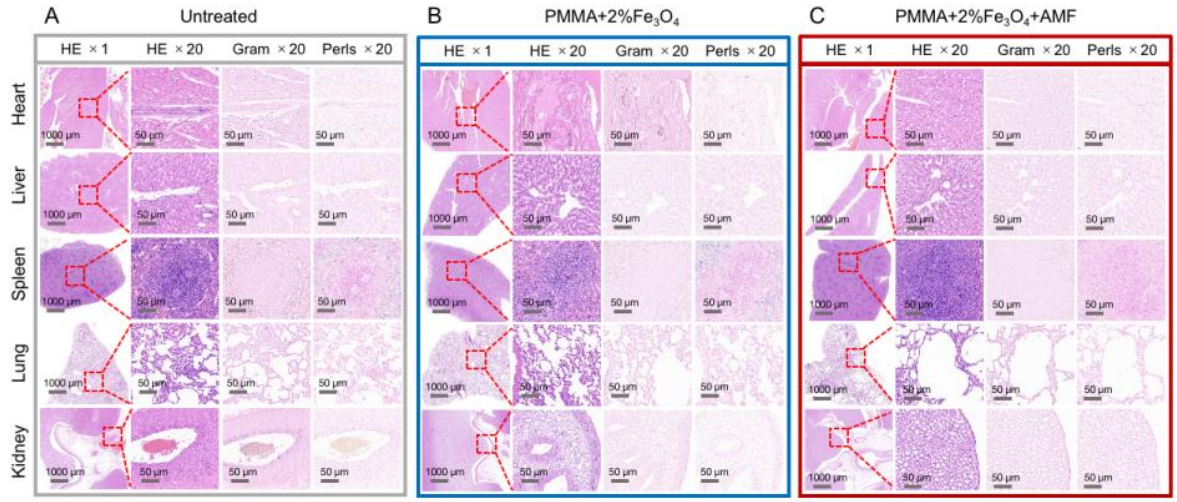

Fig. 7 No histological evidence of the iron nanoparticles releasing from PMMA+Fe_3O_4 cylinder with or without AMF application. The internal organs of the heart, liver, spleen, lung and kidney were collected for histological staining of H&E, Gram and Perls Prussian Blue to check the nanoparticles leaking or infections disseminations. There were no abnormal morphology observed in untreated (A), PMMA+2%Fe_3O_4 (B), or PMMA+2%Fe_3O_4+AMF (C) groups.

reaction or reactive new bone formation in PMMA+Fe_3O_4 group (Fig. 5B, red arrows) and cortical bone osteolysis in untreated control (Fig. 5A, yellow arrows).

The antibacterial efficiency of PMMA+2% Fe_3O_4+AMF on SIABI rabbit model was confirmed by histopathological examinations. The lower magnification of H&E staining served as reference to determine the region of interest (ROI) for the infected tibiae in untreated group (Fig. 6 A and B), PMMA+Fe_3O_4 (Fig. 6 F and G), and PMMA+Fe_3O_4+AMF group (Fig. 6 K and L), at week 7, we observed obvious leukocyte infiltration and Gram-positive cocci bacteria colonization in untreated group (Fig. 6 C and D), PMMA+ Fe_3O_4 (Fig. 6 H and I), but not in PMMA+Fe_3O_4+ AMF group (Fig. 6 M and N). This suggests that PMMA+Fe_3O_4+ AMF is effective for eradicating pathogenic bacteria from bone infection lesions. In addition, there were neither

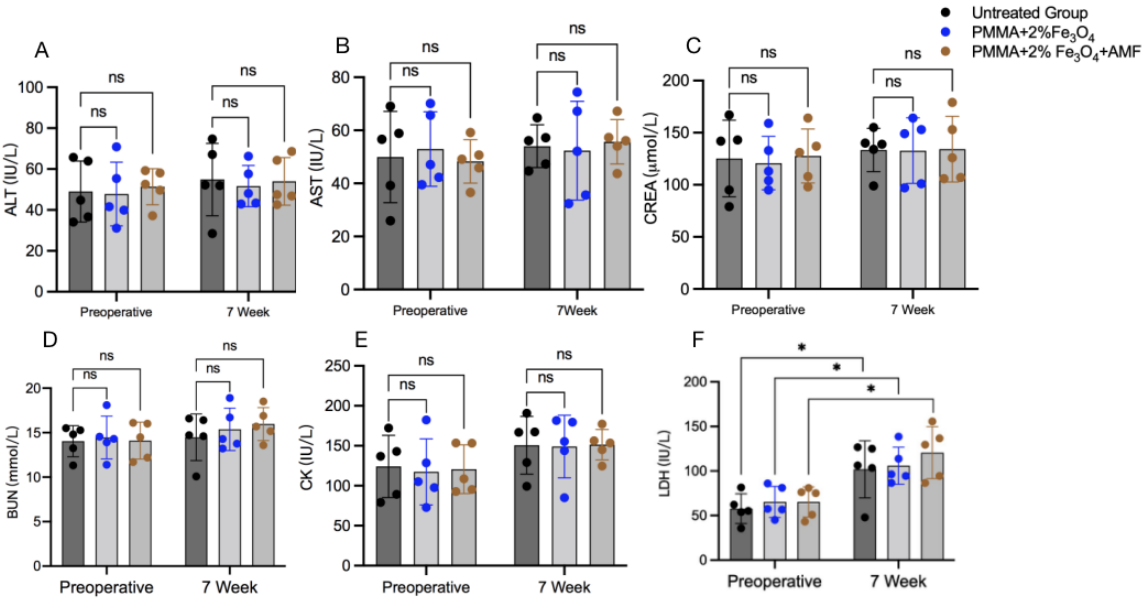

Fig. 8 Biocompatibility and Biosafety Evidence of Serological Tests of PMMA+2%Fe_3O_4. To evaluate the function of heart, liver, and kidney, serological tests of ALT, AST, CR, BUN, CK and LDH were performed and only LDH increased significantly in week 7 compared with their preoperative ($p<0.005$), but no significant difference in all three groups or between preoperative and week 7 time points were observed in rest of tests. (ns, $p>0.05$, * $p<0.05$).

noticeably tissue burns nor extra Fe_3O_4 NPs particles loaded or excessive free iron ions could be observed in the local bone tissue and medullary cavity (Fig. 6 E, J and O), which indicates the good biocompatibility and no obvious toxic effects of PMMA+Fe_3O_4 in local tissue. This was further confirmed by following Perls Prussian blue staining of histological sections of internal organ (Fig. 7).

Based on the H&E staining, Gram staining, and Prussian blue staining of the main internal organs (heart, liver, spleen, lung, and kidney) in the three experimental groups (Fig. 7), and by comparing the corresponding tissues with the untreated group, no obvious histological structural abnormalities of these organs were observed under the light microscope. Also, there were no black Fe_3O_4 particles or excessive free iron ions transferred in these viscera neither, which indicates an inability of Fe_3O_4 NPs to escape from the bone cement after the implantation of PMMA+Fe_3O_4 with or without exposure to an AMF. The serum tests evaluated the function of heart, liver and kidney (including ALT, AST, CR, BUN, CK and LDH) revealed no significant difference in all of three groups at different points (Fig. 8).

4. Discussion

The heating power of the magnetic nanoparticles depends on their magnetic features and the intensity and frequency conditions of the AMF (Gudkov *et al.* 2021). Optimizing the ratio of Fe_3O_4 NPs for PMMA+Fe_3O_4 compound cylinder is a key step to achieving a reproducible antibacterial efficiency under AMF-induced thermal temperature *in vivo* (Yang *et al.* 2017). The local temperature that leads to the microbes' death requires higher than 50^0C (Wu *et al.* 2013). The current study optimized the ratio of Fe_3O_4 NPs for PMMA + Fe_3O_4 is 2%, and under the AMF-induced temperature can reach 56^0C.

Due to the limitation of the diameter of the inner circle of the magnetocaloric working coil (3.0cm), we selected the appropriate plate with a diameter of 2.5 cm for antibacterial experiments *in vitro*, to ensure that the PMMA+2% Fe_3O_4 cylindrical locate in the center of the working coil. When PMMA+2%Fe_3O_4 cylindrical was exposed to the AMF only for 3 minutes, the antibacterial efficiency still could be observed obviously. Unfortunately, we were unable to quantitatively analyze the results of this part. Furthermore, we did not observe any antibacterial property for PMMA+ 2%Fe_3O_4 without an AMF in this research, it's distinct from other studies. (Dadfar *et al.* 2019, Gudkov *et al.* 2021)

Due to biofilm formation of *S. aureus* and colonization of the OLCN (Adjei-Sowah *et al.* 2021, Masters *et al.* 2019), recurrent and persistent infections usually occur in patients with SIABI (Kavanagh *et al.* 2018). So facing the dilemma of SIABI, we considered combining the excellent biocompatibility and magnetic properties of Fe_3O_4 NPs together (Xu *et al.* 2015, Yu *et al.* 2019) with the antibacterial potential of Fe_3O_4 NPs under the external magnetics (Gudkov *et al.* 2021, Irshad *et al.* 2017). We utilized PMMA and Fe_3O_4 NPs to establish the standard size of the PMMA+Fe_3O_4 cylinder and explored that the excellent antibacterial property of magnetic Fe_3O_4 NPs for inhibiting SIABI, accompany the biofilm formation of the pathogenic organism *in vivo*.

In this study, the mean size of the applied PMMA and Fe_3O_4 magnetic NPs were the same as in our previous studies (Yu *et al.* 2019). To match the size of the titanium screw which the tianstibial inserted into the SIABI model, we established a specific cylindrical shape of PMMA+ Fe_3O_4. The standardized size of PMMA+Fe_3O_4 NPs

cylinder could receive magnetic-thermal-induced thermal conversion under an AMF that achieves the temperature of antibacterial in vivo. In order to determine the distance of heat penetration to adjacent bone and soft tissue, we performed the Rearranged Fourier's Heat Transfer Equation to solve the diameter of the heat range. We found that under the current AMF condition, to maintain the temperature of PMMA+2% Fe_3O_4 cylinder at 56^0C, and the temperature of the bone-soft boundary at 50^0C, the distance of heat penetration is around 68.15um, which is an idea range to cover *S. aureus* colonized within OLCN. Some other research has illustrated that 45 °C causes no damage to normal tissues (Xu *et al*. 2018), although light high temperature (70 °C) was essential for effectively killing of bacteria, but would also damage nearby nontarget cells or tissues (Fan *et al*. 2019). Therefore, considering the results of biomechanical testing and the magnetic-thermal-induced thermal efficiency together, we finally selected PMMA+2% Fe_3O_4 for the following experimental in this project.

Based on the CFU assay data on week 7, we found that the PMMA+Fe_3O_4+AMF group could reduce the number of bacteria in the infected lesions effectively, and there was a statistically significant difference when compared with the other two groups. However, on week 7, the removal implants from the rabbit of PMMA+Fe_3O_4+AMF group still could isolate out bacteria, we considered that the contamination or migration of organisms which colonization in the adjacent infectious soft tissue might be responsible for this phenomenon. We even removed the infectious screws from the wound on week 1, which means only debridement may not enough to remove pathogenic organisms from infected lesions completely, and that's one of main reasons for causing recurrent of osteomyelitis as previous studies mentioned (Fu *et al*. 2021, Saeed *et al*. 2019).

To our best knowledge, CT image features, like extensive osteolysis and bone resorption, periosteal reaction, and formation of reactive new bone could be observed when with SIABI (Chu *et al*. 2020, Diaz-Ledezma *et al*. 2019, Jacquier *et al*. 2004, Stadelmann *et al*. 2020). Although it is well known that foreign implants can also cause local periosteal reactions, it rarely causes the formation of reactive new bone (Stadelmann *et al*. 2020). Fortunately, here we did not observe similar periosteal reactions in the PMMA+Fe_3O_4+AMF group, so is it possible that the periosteal reaction and formation of reactive new bone in the PMMA+Fe_3O_4 group was mainly caused by *S.aureus*. Taking all these findings of CT images into account, we did not observe any signals of bone resorption, bone defect, and periosteal reaction in CT images of the PMMA+Fe_3O_4H group, which strongly provides evidence for that the PMMA+Fe_3O_4 compound can treat SIABI directly. Some previous studies showed that Fe_3O_4 NPs have less-pronounced cytotoxic properties and good biocompatibility in vivo and in vitro (Gudkov *et al*. 2021, Hanini *et al*. 2011). In this project, although the Perls Prussian blue stained section of bone tissue in the untreated group showed that there were relatively few golden yellow areas in the region of interest than others, we need to declare that it may depend on the region of interest which we selected, because Perls Prussian blue staining could show iron ions loaded when only osteomyelitis occurs as well (Bierry *et al*. 2008). Therefore, using the size of the golden yellow area in the image to judge the therapeutic effect may not be completely accurate. It is essential to combine the condition of extra Fe_3O_4 NPs particles loaded and the influence of iron ions on osteocytes like other studies mentioned (Shi *et al*. 2012).

The limitations of this study: 1) Even though facing the limited characteristics of the non-degradability and non-flowability of PMMA+ Fe_3O_4, this study still can achieve the goal that eradicating the bacteria within the biofilms formation and colonization in the OLCN through the magnetothermal efficiency of Fe_3O_4 NPs in an AMF, what's pity is that this study does not provide the strong evidence about the physiopathological reactive characteristics on the interface of material-infectious tissue and proof of layer-by-layer gradient death of pathogenic bacteria around the material due to thermal effects neither, but that would be the focus of our future research. 2) Up to now, large numbers of literatures noted that Fe_3O_4 NPs have less-pronounced cytotoxic properties and good biocompatibility both in vivo and *in vitro* (Gudkov *et al*. 2021, Qiao *et al*. 2020), and based on the sufficient evidence for the biosafety and biocompatibility of Fe_3O_4 NPs in our previous studies demonstrated (Liang *et al*. 2019, 2020, Wang *et al*. 2017, Yu *et al*. 2019), so here we did not perform too much cytotoxicity experiment for Fe_3O_4 NPs in vivo and in ex vivo, but the phenomenon of ectopic transfer of iron ions to the adjacent bone tissue and internal organs or the burning injury of normal tissues were not definitely observed in this study. However, we realized that the response characteristics of the osteoimmunology in the infectious microenvironment which caused by the magnetic nanomaterial itself and the magnetocaloric effect are still unclear, and whether those kinds of changes have probably long-term and potential side effects should not be negligible in the following research. 3) As our previous study demonstrated (Chu *et al*. 2020, Fu *et al*. 2021, Peng *et al*. 2017), there are many serological testing indicators for diagnosing or evaluating the severity of bone infections, even the combination of multiple serological indicators is usually required but not compulsory (Chu *et al*. 2020). In this study, due to the limitation of reagents, we only examined the white blood cell count, but the results of histopathology, it's the gold standard for evaluating the severity of SIABI, so this is not inconsistent with our previous research. Meanwhile, we noticed that with reduced graphene oxide (rGO) as a carrier combined with functionalization of Fe_3O_4 NPs, the thermal-induced photon ablation will be enhanced, and further studies are pending (Karvelas *et al*. 2021, Yulia R. Mukhortova 2022).

5. Conclusions

Under magnetic-thermal-induced thermal conversion in an AMF, PMMA+Fe_3O_4 displayed the excellent anti-bacterial property for SIABI, especially with the biofilm formation of pathogenic organism *in vivo*. Basing on the

outstanding biomechanical properties of PMMA, the low toxicity and less-pronounced cytotoxic of Fe_3O_4 magnetic nanomaterials. PMMA+Fe_3O_4 might provide an alternative novel sight into the treatment of SIABI.

Acknowledgments

Dr.Youliang Ren and Dr. Jin Yang contributed equally to this article as the co-first author. This work was supported by the Fellowship of China Postdoctoral Science Foundation (2021M693758) and Natural Science Foundation Postdoctoral Science Foundation Project of Chongqing (cstc2021jcyj-bsh0019). We are grateful to acknowledge Thomas Xue (University of Rochester, Rochester, USA) for proofreading this manuscript. Dr. Jing Zhang (Department of Hematology, Shanghai Tongren Hospital) for assistance with statistical analysis.

References

Adjei-Sowah, E., Peng, Y., Weeks, J., Jonason, J.H., de Mesy Bentley, K.L., Masters, E., Morita, Y., Muthukrishnan, G., Cherian, P., Hu, X.E., McKenna, C.E., Ebetino, F.H., Sun, S., Schwarz, E.M. and Xie, C. (2021), "Development of bisphosphonate-conjugated antibiotics to overcome pharmaco-dynamic limitations of local therapy: Initial results with carbamate linked sitafloxacin and tedizolid", *Antibiotics*, **10**. https://doi.org/10.3390/antibiotics10060732.

Bierry, G., Jehl, F., Boehm, N., Robert, P., Prevost, G., Dietemann, J.L., Desal, H. and Kremer, S. (2008), "Macrophage activity in infected areas of an experimental vertebral osteomyelitis model: USPIO-enhanced MR imaging--feasibility study", *Radiology*, **248**, 114-23. https://doi.org/10.1148/radiol.2481071260.

Chen, Y., Jiang, L., Wang, R., Lu, M., Zhang, Q., Zhou, Y., Wang, Z., Lu, G., Liang, P., Ran, H., Chen, H. and Zheng, Y. (2014), "Injectable smart phase-transformation implants for highly efficient in vivo magnetic-hyperthermia regression of tumors", *Adv Mater*, **26**, 7468-7473. https://doi.org/10.1002/adma.201402509.

Chu, L., Ren, Y.L., Yang, J.S., Yang, J., Zhou, H., Jiang, H.T., Shi, L., Hao, D.J. and Deng, Z.L. (2020), "The combinations of multiple factors to improve the diagnostic sensitivity and specificity after artificial joint infection", *J. Orthop. Surg. Res.*, **15**, 161. https://doi.org/10.1186/s13018-020-01669-8.

Dadfar, S.M., Roemhild, K., Drude, N.I., von Stillfried, S., Knuchel, R., Kiessling, F. and Lammers, T. (2019), "Iron oxide nanoparticles: Diagnostic, therapeutic and theranostic applications", *Adv. Drug Deliv. Rev.*, **138**, 302-325. https://doi.org/10.1016/j.addr.2019.01.005.

Diaz-Ledezma, C., Espinosa-Mendoza, R., Gallo, J., Glaudemans, A., Gómez-García, F., Goodman, S., Kaminek, M., Le Roux, T. L.B., Llinás, A., Nieslanikova, E., Quinn, L., Sculco, P. and Svoboda, M. (2019), "General assembly, diagnosis, imaging: Proceedings of international consensus on orthopedic infections", *J. Arthroplasty*, **34**, S215-223. https://doi.org/10.1016/j.arth.2018.09.073.

Fan, X.L., Li, H.Y., Ye, W.Y., Zhao, M.Q., Huang, D.N., Fang, Y., Zhou, B.Q., Ren, K.F., Ji, J. and Fu, G.S. (2019), "Magainin-modified polydopamine nanoparticles for photothermal killing of bacteria at low temperature", *Colloid Surface B*, **183**, 110423. https://doi.org/10.1016/j.colsurfb.2019.110423.

Fu, W., He, W., Ren, Y., Li, Z., Liu, J., Liu, Y., Xie, Z., Xu, J., Bi, Q., Kong, M., Lee, C.C., Daiss, J.L., Muthukrishnan, G., Owen, J.R., Kates, S.L., Peng, J. and Xie, C. (2021), "Distinct expression trend of signature antigens of Staphylococcus aureus osteomyelitis correlated with clinical outcomes", *J. Orthop. Res.*, **39**, 265-273. https://doi.org/10.1002/jor.24961.

Gudkov, S.V., Burmistrov, D.E., Serov, D.A., Rebezov, M.B., Semenova, A.A. and Lisitsyn, A.B. (2021), "Do iron oxide nanoparticles have significant antibacterial properties?", *Antibiotics*, **10**. https://doi.org/10.3390/antibiotics10070884.

Hanini, A., Schmitt, A., Kacem, K., Chau, F., Ammar, S. and Gavard, J. (2011), "Evaluation of iron oxide nanoparticle biocompatibility", *Int. J. Nanomed.*, **6**, 787-794. https://doi.org/10.2147/IJN.S17574.

Irshad, R., Tahir, K., Li, B., Ahmad, A.A.R.S. and Nazir, S. (2017), "Antibacterial activity of biochemically capped iron oxide nanoparticles: A view towards green chemistry", *J. Photochem. Photobiol. B*, **170**, 241-246. https://doi.org/10.1016/j.jphotobiol.2017.04.020.

Jacquier, A., Champsaur, P., Vidal, V., Stein, A., Monnet, O., Drancourt, M., Argenson, J.N., Raoult, D., Moulin, G. and Bartoli, J.M. (2004), "CT evaluation of total HIP prosthesis infection", *J. Radiol.*, **85**, 2005-2012. https://doi.org/10.1016/s0221-0363(04)97773-6.

Karvelas, E.G., Lampropoulos, N.K., Benos, L.T., Karakasidis, T. and Sarris, I.E. (2021), "On the magnetic aggregation of Fe_3O_4 nanoparticles", *Comput. Meth. Prog. Bio.*, **198**, 105778. https://doi.org/10.1016/j.cmpb.2020.105778.

Kavanagh, N., Ryan, E.J., Widaa, A., Sexton, G., Fennell, J., O'Rourke, S., Cahill, K.C., Kearney, C.J., O'Brien, F.J. and Kerrigan, S.W. (2018), "Staphylococcal osteomyelitis: Disease progression, treatment challenges and future directions", *Clin. Microbiol. Rev.*, **31**. https://doi.org/10.1128/CMR.00084-17.

Leiblein, M., Koch, E., Winkenbach, A., Schaible, A., Nau, C., Büchner, H., Schröder, K., Marzi, I. and Henrich, D. (2020), "Size matters: Effect of granule size of the bone graft substitute (Herafill®) on bone healing using Masquelet's induced membrane in a critical size defect model in the rat's femur", *J. Biomed. Mater. Res. B Appl. Biomater.*, **108**, 1469-1482. https://doi.org/10.1002/jbm.b.34495.

Liang, B., Yu, K., Ling, Y., Kolios, M., Exner, A., Wang, Z., Hu, B., Zuo, G., Chen, Y. and Zheng, Y. (2019), "An artificially engineered "tumor bio-magnet" for collecting blood-circulating nanoparticles and magnetic hyperthermia", *Biomater. Sci.*, **7**, 1815-1824. https://doi.org/10.1039/c8bm01658e.

Liang, B., Zuo, D., Yu, K., Cai, X., Qiao, B., Deng, R., Yang, J., Chu, L., Deng, Z., Zheng, Y. and Zuo, G. (2020), "Multifunctional bone cement for synergistic magnetic hyperthermia ablation and chemotherapy of osteosarcoma", *Mater. Sci. Eng. C Mater. Biol. Appl.*, **108**, 110460. https://doi.org/10.1016/j.msec.2019.110460.

Liu, G., Gao, J., Ai, H. and Chen, X. (2013), "Applications and potential toxicity of magnetic iron oxide nanoparticles", *Small*, **9**, 1533-1545. https://doi.org/10.1002/smll.201201531.

Masters, E.A., Trombetta, R.P., de Mesy Bentley, K.L., Boyce, B.F., Gill, A.L., Gill, S.R., Nishitani, K., Ishikawa, M., Morita, Y., Ito, H., Bello-Irizarry, S.N., Ninomiya, M., Brodell, J.D., Jr., Lee, C.C., Hao, S.P., Oh, I., Xie, C., Awad, H.A., Daiss, J.L., Owen, J.R., Kates, S.L., Schwarz, E.M. and Muthukrishnan, G. (2019), "Evolving concepts in bone infection: Redefining "biofilm", "acute vs. chronic osteomyelitis", "the immune proteome" and "local antibiotic therapy"", *Bone Res.*, **7**, 20. https://doi.org/10.1038/s41413-019-0061-z.

Patel, A., Pavlou, G., Mújica-Mota, R. E. and Toms, A. D. (2015), "The epidemiology of revision total knee and hip arthroplasty in England and Wales: A comparative analysis with projections for the United States, A study using the National Joint Registry dataset", *Bone Joint J.*, **97-b**, 1076-1081. https://doi.org/10.1302/0301-620x.97b8.35170.

Peng, J., Ren, Y., He, W., Li, Z., Yang, J., Liu, Y., Zheng, Z., Kates, S.L., Schwarz, E.M., Xie, C. and Xu, Y. (2017), "Epidemiological, clinical and microbiological characteristics of patients with post-traumatic osteomyelitis of limb fractures in southwest china: A hospital-based study", *J. Bone Joint Infect*, **2**, 149-153. https://doi.org/10.7150/jbji.20002.

Qiao, Y., Liu, X., Li, B., Han, Y., Zheng, Y., Yeung, K.W.K., Li, C., Cui, Z., Liang, Y., Li, Z., Zhu, S., Wang, X. and Wu, S. (2020), "Treatment of MRSA-infected osteomyelitis using bacterial capturing, magnetically targeted composites with microwave-assisted bacterial killing", *Nat. Commun.*, **11**, 4446. https://doi.org/10.1038/s41467-020-18268-0.

Saeed, K., McLaren, A.C., Schwarz, E.M., Antoci, V., Arnold, W.V., Chen, A.F., Clauss, M., Esteban, J., Gant, V., Hendershot, E., Hickok, N., Higuera, C.A., Coraca-Huber, D.C., Choe, H., Jennings, J.A., Joshi, M., Li, W.T., Noble, P.C., Phillips, K.S., Pottinger, P.S., Restrepo, C., Rohde, H., Schaer, T.P., Shen, H., Smeltzer, M., Stoodley, P., Webb, J.C.J. and Witso, E. (2019), "2018 international consensus meeting on musculoskeletal infection: Summary from the biofilm workgroup and consensus on biofilm related musculoskeletal infections", *J. Orthop. Res.*, **37**, 1007-1017. https://doi.org/10.1002/jor.24229.

Shi, S.F., Jia, J.F., Guo, X.K., Zhao, Y.P., Chen, D.S., Guo, Y.Y., Cheng, T. and Zhang, X.L. (2012), "Biocompatibility of chitosan-coated iron oxide nanoparticles with osteoblast cells", *Int. J. Nanomed.*, **7**, 5593-5602. https://doi.org/10.2147/IJN.S34348.

Shi, S.F., Jia, J.F., Guo, X.K., Zhao, Y.P., Chen, D.S., Guo, Y.Y. and Zhang, X.L. (2016), "Reduced Staphylococcus aureus biofilm formation in the presence of chitosan-coated iron oxide nanoparticles", *Int. J. Nanomed.*, **11**, 6499-6506. https://doi.org/10.2147/IJN.S41371.

Stadelmann, V.A., Thompson, K., Zeiter, S., Camenisch, K., Styger, U., Patrick, S., McDowell, A., Nehrbass, D., Richards, R.G. and Moriarty, T.F. (2020), "Longitudinal time-lapse in vivo micro-CT reveals differential patterns of peri-implant bone changes after subclinical bacterial infection in a rat model", *Sci. Rep.*, **10**, 20901. https://doi.org/10.1038/s41598-020-77770-z.

Tian, X., Zhang, L., Yang, M., Bai, L., Dai, Y., Yu, Z. and Pan, Y. (2018), "Functional magnetic hybrid nanomaterials for biomedical diagnosis and treatment", *Wiley Interdiscip. Rev. Nanomed. Nanobiotechnol.*, **10**. https://doi.org/10.1002/wnan.1476.

Wang, F., Yang, Y., Ling, Y., Liu, J., Cai, X., Zhou, X., Tang, X., Liang, B., Chen, Y., Chen, H., Chen, D., Li, C., Wang, Z., Hu, B. and Zheng, Y. (2017), "Injectable and thermally contractible hydroxypropyl methyl cellulose/Fe_3O_4 for magnetic hyperthermia ablation of tumors", *Biomaterials*, **128**, 84-93. https://doi.org/10.1016/j.biomaterials.2017.03.004.

Weissleder, R., Stark, D.D., Engelstad, B.L., Bacon, B.R., Compton, C.C., White, D.L., Jacobs, P. and Lewis, J. (1989), "Superparamagnetic iron oxide: Pharmacokinetics and toxicity", *AJR Am. J. Roentgenol*, **152**, 167-173. https://doi.org/10.2214/ajr.152.1.167.

Wu, M.C., Deokar, A.R., Liao, J.H., Shih, P.Y. and Ling, Y.C. (2013), "Graphene-based photothermal agent for rapid and effective killing of bacteria", *ACS Nano*, **7**, 1281-1290. https://doi.org/10.1021/nn304782d.

Xu, C., Zheng, Y., Gao, W., Xu, J., Zuo, G., Chen, Y., Zhao, M., Li, J., Song, J., Zhang, N., Wang, Z., Zhao, H. and Mei, Z. (2015), "Magnetic hyperthermia ablation of tumors using injectable Fe_3O_4/Calcium phosphate cement", *ACS Appl. Mater. Interf.*, **7**, 13866-75. https://doi.org/10.1021/acsami.5b02077.

Xu, X., Liu, X., Tan, L., Cui, Z., Yang, X., Zhu, S., Li, Z., Yuan, X., Zheng, Y., Yeung, K.W.K., Chu, P. K. and Wu, S. (2018), "Controlled-temperature photothermal and oxidative bacteria killing and acceleration of wound healing by polydopamine-assisted Au-hydroxyapatite nanorods", *Acta Biomater*, **77**, 352-364. https://doi.org/10.1016/j.actbio.2018.07.030.

Yang, Y., He, P., Wang, Y., Bai, H., Wang, S., Xu, J. F. and Zhang, X. (2017), "Supramolecular radical anions triggered by bacteria in situ for selective photothermal therapy", *Angew Chem. Int. Ed. Engl.*, **56**, 16239-16242. https://doi.org/10.1002/anie.201708971.

Yu, K., Liang, B., Zheng, Y., Exner, A., Kolios, M., Xu, T., Guo, D., Cai, X., Wang, Z., Ran, H., Chu, L. and Deng, Z. (2019), "PMMA-Fe_3O_4 for internal mechanical support and magnetic thermal ablation of bone tumors", *Theranostics*, **9**, 4192-4207. https://doi.org/10.7150/thno.34157.

Yulia R. Mukhortova, A.S.P., Roman V. Chernozem, Igor O. Pariy, Elizaveta A. Akoulina, Irina V. Demianova, Irina I. Zharkova, Yurii F. Ivanov, Dmitriy V. Wagner, Anton P. Bonartsev, Roman A. Surmenev, Maria A. Surmeneva, (2022), "Fabrication and characterization of a magnetic biocomposite of magnetite nanoparticles and reduced graphene oxide for biomedical applications", *Nano Struct. Nano Objects*, **29**. https://doi.org/2352-507X.

JL